Characterization of Erythromycin Analogs by Collisional Activated Dissociation and Infrared Multiphoton Dissociation in a Quadrupole Ion Trap

Matthew C. Crowe and Jennifer S. Brodbelt
Department of Chemistry and Biochemistry, University of Texas at Austin, Austin, Texas, USA

Brian J. Goolsby
Motorola DigitalDNA Laboratories, Austin, Texas, USA

Paul Hergenrother
Department of Chemistry, University of Illinois, Urbana, Illinois, USA

The effectiveness of two activation techniques, collision activated dissociation (CAD) and infrared multiphoton dissociation (IRMPD), is compared for structural characterization of protonated and lithium-cationized macrolides and a series of synthetic precursors in a quadrupole ion trap (QIT). Generally, cleavage of the glycosidic linkages attaching the sugars to the macrolide ring and water losses constitute the major fragmentation pathways for most of the protonated compounds. In the IRMPD spectra, a diagnostic fragment ion assigned as the desosamine ion is a dominant ion that is not observed in the CAD spectra because of the higher *m/z* limit of the storage range required during collisional activation. Activation of the lithium-cationized species results in new diagnostic fragmentation pathways that are particularly useful for confirming the identities of the protecting groups in the synthetic precursors. Multi-step IRMPD allows mapping of the fragmentation genealogies in greater detail and supports the proposed structures of the fragment ions. (J Am Soc Mass Spectrom 2002, 13, 630–649) © 2002 American Society for Mass Spectrometry

Interest in the analysis of macrolide antibiotics has grown in recent years as new compounds, resulting from the manipulation of the biosynthetic pathways of *Streptomyces* bacteria, may offer improved activities against antibiotic-resistant bacteria [1]. Novel analogs of macrolide compounds are also produced from modifications of erythromycin during attempts at total synthesis [2]. The clinical testing of these erythromycin analogs for bacteriostatic potential, possible human toxicity, and pharmacokinetics requires effective analytical techniques. Mass spectrometry has been utilized in several recent studies aimed at identifying the structures and fragmentation pathways of macrolide antibiotics [3–9]. For example, Gross and co-workers used fast atom bombardment (FAB) to create both protonated and alkali metal cationized species of erythromycin A, megalomicin A, desmycosin, megalalosamine, and tylosin, followed by CAD for structural characterization [3]. They noted that the protonated macrolides gave fragmentation patterns that lacked mid-range fragment ions, whereas the alkali metal cationized species gave a greater variety of fragment ions. Gates et al. used isotopic labeling to determine the origin of the initial water loss from protonated erythromycin [4, 5]. For these studies, electrospray ionization (ESI) was used to introduce samples into either a Fourier transform ion cyclotron resonance (FTICR) mass spectrometer (for accurate mass measurements), a quadrupole-time-of-flight (Q-TOF) instrument, or a quadrupole ion trap for MS/MS experiments. Based on the ^{18}O-labeling, it was found that the first loss of water occured from the C-9 carbonyl group, indicating that the carbonyl oxygen was protonated, not the more basic amine group in the desosamine moiety. They also confirmed via MS^n experiments that the first macrolide ring cleavage involved the C-13 position and adjacent oxygen, with the net loss identified as a substituted ketone moiety [4]. Volmer and Hui incubated erythromycin in aqueous solutions at non-physiological pH [6], and subsequently

Published online April 22, 2002

Address reprint requests to Dr. J. S. Brodbelt, Department of Chemistry and Biochemistry, University of Texas at Austin, Austin, TX 78712-1167, USA. E-mail: jbrodbelt@mail.utexas.edu

1044-0305/02/$20.00
PII S1044-0305(02)00366-5

Received November 30, 2001
Revised January 25, 2002
Accepted January 25, 2002

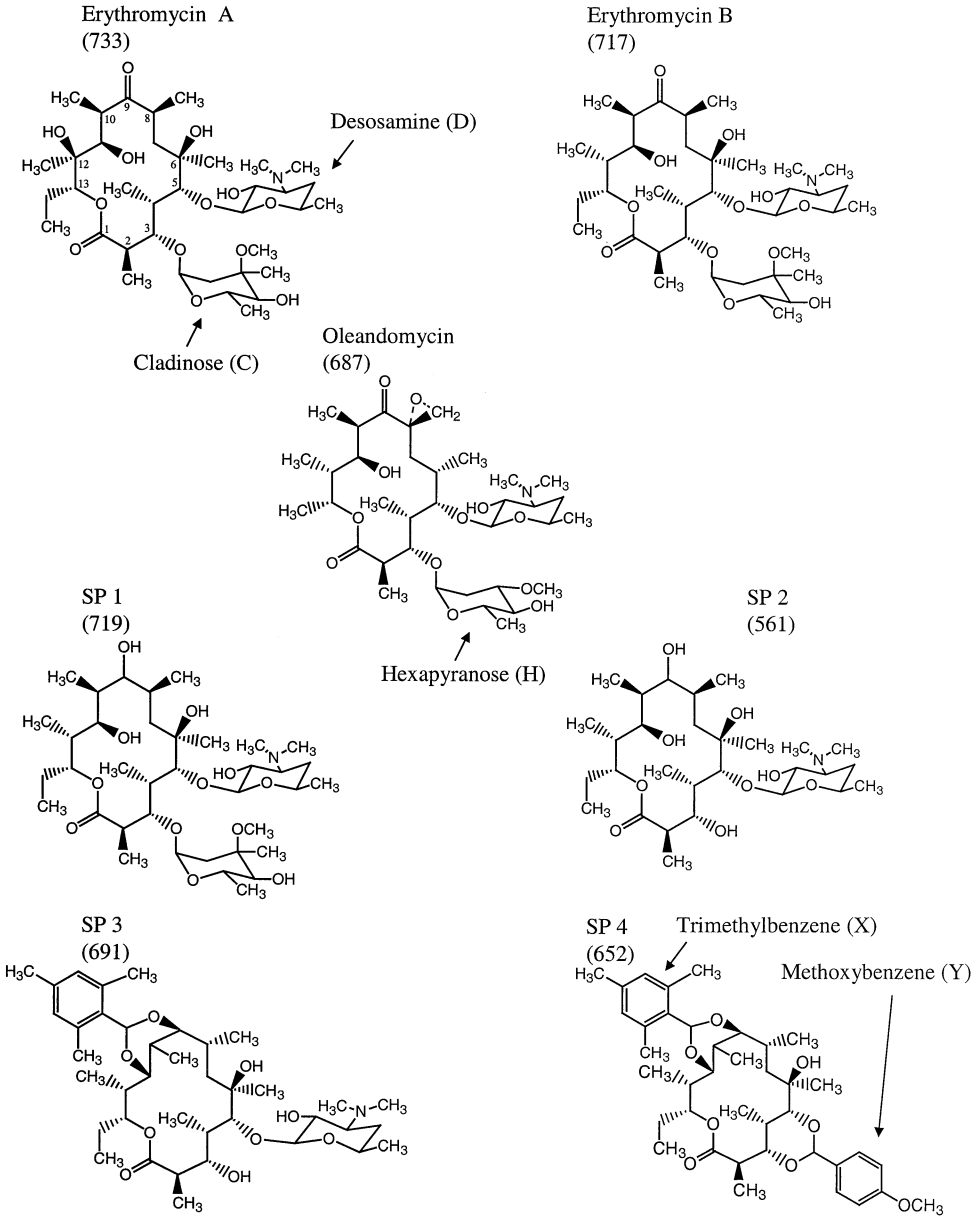

Figure 1. Structures of macrolides (molecular weight in Da).

used solid phase microextraction/high performance liquid chromatography/ESI-MS to determine the decomposition products of protonated erythromycin in a triple quadrupole mass spectrometer. Ling et al. demonstrated the use of matrix assisted laser desorption ionization (MALDI) TOF-MS to quantify numerous classes of antibiotics, including macrolides, from methanol solutions using an internal standard [9].

The structural characterization of macrolides by mass spectrometry has proven to be an ongoing analytical challenge because of the low number of diagnostic fragment ions in the CAD spectra of the protonated molecules. For example, protonated macrolides typically lose water molecules in succession as the dominant dissociation pathways [5]. Another recognized feature of the dissociation behavior of protonated macrolides is their tendency to lose their sugar functional groups while the large, flexible macrolide ring remains largely intact. Confirmation of the type of sugars or other substituents at carbons 3, 5, and 11 (Figure 1) is a key issue in the characterization of new analogs. The use of other activation and ionization methods may provide an avenue for addressing the challenging structural characterization problems associated with the analysis of macrolides.

In the present study, CAD and IRMPD are used to characterize three macrolide compounds and four precursors of an in vitro total synthesis of erythromycin B (Figure 1). Lithium cationization was also evaluated as a potential means of providing complementary structural information obtained from fragmentation. Alkali metal cationization in general has been explored in

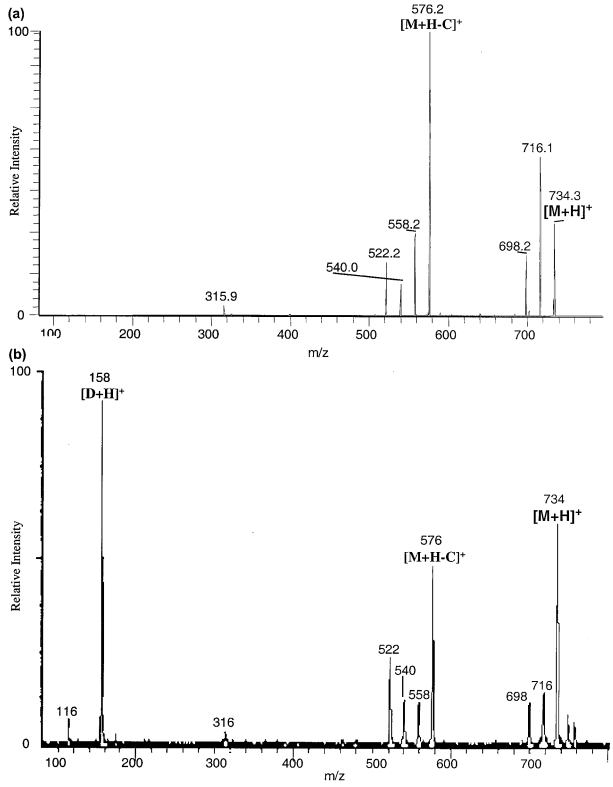

Figure 2. (**a**) CAD and (**b**) IRMPD of protonated erythromycin A.

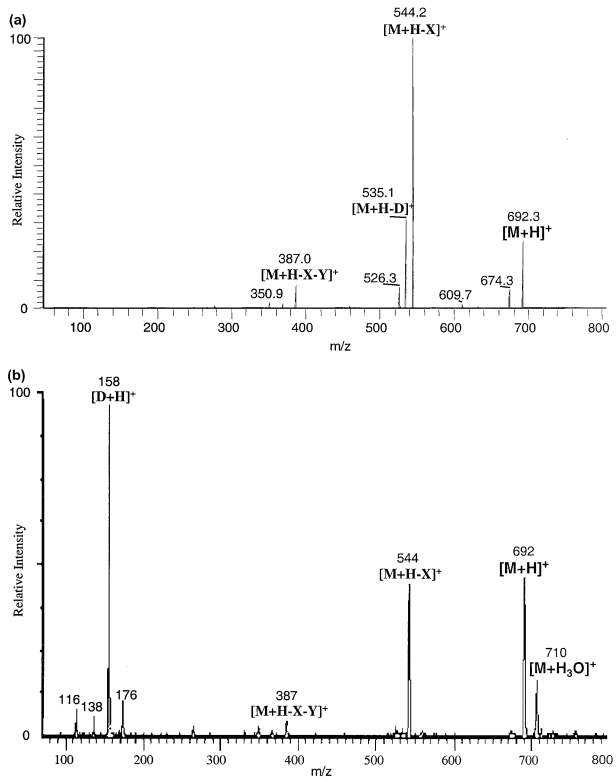

Figure 3. (**a**) CAD and (**b**) IRMPD of protonated SP3.

recent years as an alternative to conventional protonation in electrospray ionization and as a means to change the sites of charge localization and promote different fragmentation processes [10–15]. In this report, the fragmentation promoted by CAD and IRMPD methods (including multi-stage tandem mass spectrometry [MS^n]) is compared, along with an evaluation of the diagnostic utility of the fragmentation patterns obtained from the protonated versus lithium-cationized macrolides. A focal point was to determine the best manner for confirming the substituents (i.e., protecting groups and/or sugars for the synthetic precursors) present in the macrolides that would allow confident identification of the structures.

Infrared multiphoton dissociation has been shown to be a viable alternative to CAD for probing molecular structures in trapping instruments [16–29]. In some cases, IRMPD proves to be more efficient than CAD, making it more suitable for MS^n experiments. This advantage results from the fact that IRMPD does not appreciably alter the kinetic energy or stable orbits of the trapped ions. Collisional techniques, however, may lead to ion scattering during energetic collisions intended to excite them internally. Furthermore, in quadrupole ion traps, IRMPD is effective regardless of the trapping potential applied to the ring electrode. Thus, the low-mass cut-off can be maintained at a sufficiently low level that fragments over a wide mass range can be stored and detected. For example, the most effective CAD conditions typically allow trapping of fragment ions that have mass-to-charge values that are at least 33% of that of the precursor ion, whereas the IRMPD conditions allow storage of fragment ions that might have mass-to-charge values that are only 10% of the mass-to-charge of the parent ion. The possibility of performing MS^n by using discreet states of irradiation and isolation can be advantageous for probing genealogies of dissociation while maintaining highly efficient trapping conditions. One potential downside of IRMPD is that activation is less efficient at higher pressures because of the competition from collisional cooling; however, trapping is less effective at lower pressures. A strategy for alleviating this trade-off has been reported recently by the combination of IRMPD with heating of the trap, thus improving energy deposition while maintaining satisfactory trapping efficiency by allowing use of higher pressures [29]. Although not used in the present application because of the naturally high dissociation efficiencies of the erythromycin compounds, heating should offset this drawback of IRMPD for other applications.

Experimental

Two QIT mass spectrometers with electrospray ionization sources were used. The first instrument was an in-house built QIT system that utilized modified Finnigan ITD electronics and software with an ESI source

Table 1. CAD and IRMPD data for protonated molecules

Compound	Parent (*m/z*)	Fragments (*m/z*)	Neutral loss	CAD Results Percent	IRMPD Results Percent
Erythromycin A	734	716	18	24%	6%
		698	36	9%	6%
		576	158	41%	21%
		558	176	11%	6%
		540	194	5%	6%
		522	212	8%	10%
		316	418	2%	2%
		158	576	—	40%
		116	620	—	3%
Erythromycin B	718	700	18	38%	12%
		560	158	22%	11%
		542	176	10%	8%
		524	194	27%	57%
		316	402	3%	1%
		158	560	—	10%
		116	604	—	1%
Oleandomycin	688	616	72	2%	—
		544	144	86%	42%
		387	301	1%	—
		369	319	2%	—
		351	337	1%	—
		302	386	8%	—
		158	530	—	54%
		116	572	—	4%
SP1	720	702	128	1%	—
		562	158	97%	42%
		544	176	1%	2%
		316	404	1%	1%
		176	544	—	2%
		158	562	—	49%
		116	606	—	4%
SP2	562	544	18	62%	3%
		405	157	8%	—
		387	175	5%	1%
		369	193	2%	—
		351	211	3%	2%
		267	295	6%	2%
		176	386	2%	3%
		158	404	12%	75%
		138	424	—	2%
		116	448	—	12%
SP3	692	674	18	4%	1%
		610	82	1%	—
		544	148	62%	24%
		535	157	20%	1%
		526	166	5%	2%
		517	175	<1%	<1%
		387	305	5%	2%
		369	323	1%	1%
		351	341	1%	2%
		267	425	1%	2%
		176	516	—	6%
		158	534	—	53%
		138	554	—	3%
		116	578	—	4%
SP4	653	635	18	1%	1%
		517	136	64%	13%

(continued)

Table 1. Continued

Compound	Parent (*m/z*)	Fragments (*m/z*)	Neutral loss	CAD Results Percent	IRMPD Results Percent
		505	148	3%	1%
		487	166	2%	4%
		369	284	13%	13%
		351	302	13%	29%
		333	320	2%	9%
		—	387	—	5%
		241	412	2%	7%
		—	429	—	9%
		—	533	—	9%

and interface modeled after the Oak Ridge National Laboratory design [30]. A stored waveform inverse Fourier transform (SWIFT) system controlled by TTL triggers in the scan function was used for resonant ejection and was described in detail previously [17]. IRMPD experiments were performed with a model 575 Apollo (Apollo Lasers, Chatsworth, CA) continuous-wave CO_2 laser used in conjunction with a Uniblitz shutter (Vincent Associates, Rochester, NY). The center of the trap was irradiated through a ZnSe window (II-VI Incorporated Saxonburg, PA) in the vacuum chamber aligned with a 6 mm hole drilled radially in the ring electrode [17]. The IRMPD laser irradiation was varied between 1 and 1000 ms as needed at a flux of 45 W/cm^2.

For the IRMPD experiments, solutions of each macrolide were made up in methanol at concentrations of 5×10^{-4} M. For lithium complexation experiments, equal volumes of 5×10^{-3} M metal salt solution and aminoglycoside solution were combined to provide a 10 times metal excess. Electrospray of the solutions was undertaken at a needle voltage of 4.0 kV and a flow rate of 3 uL/min. The chamber pressure was typically 0.1 mtorr (uncorrected) based on the mixture of air and solvent admitted through the ESI orifice; addition of an auxiliary bath gas was unnecessary. Note that this

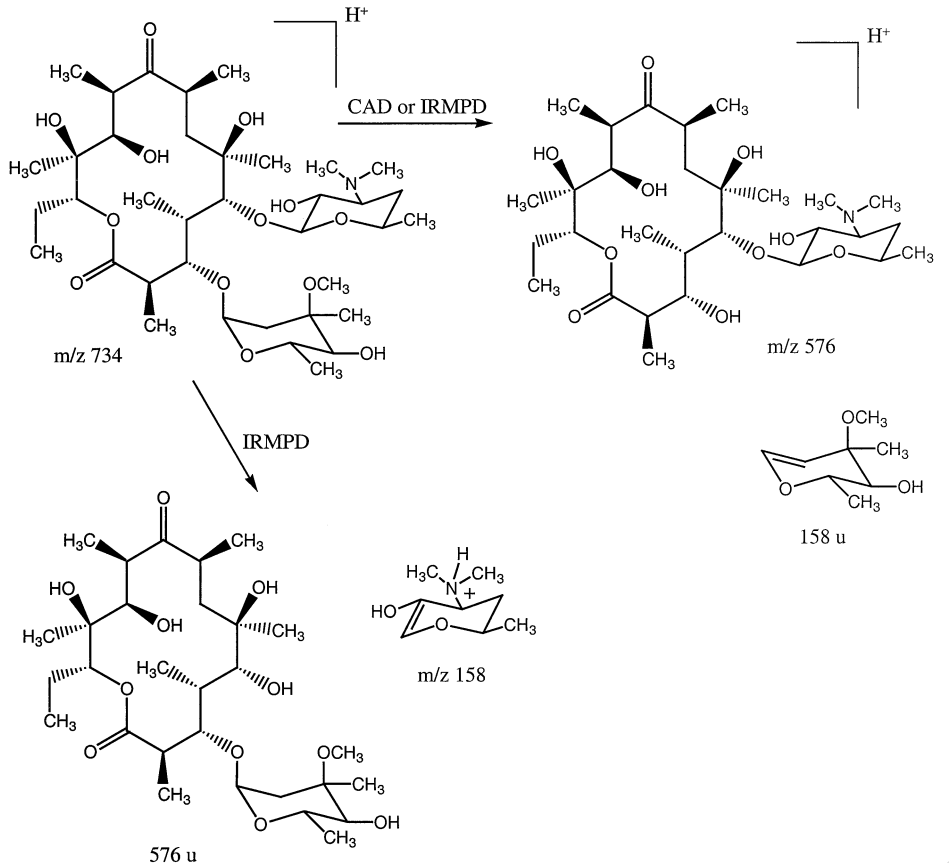

Scheme 1

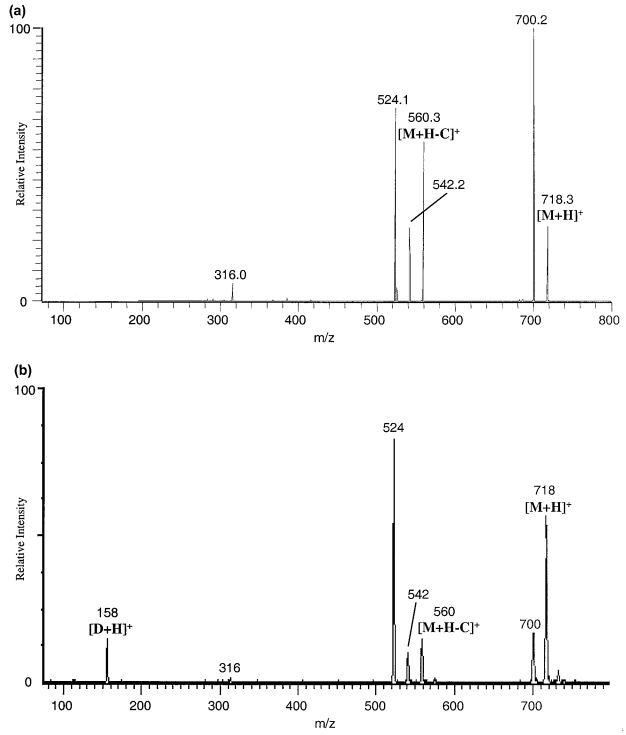

Figure 4. (**a**) CAD and (**b**) IRMPD of protonated erythromycin B.

pressure is so high that helium is never routinely added to this system, even for CAD experiments. This is clearly an artifact of the ESI interface design, and other ESI/quadrupole ion trap systems typically require the use of helium to improve trapping efficiencies.

CAD experiments were performed on a Finnigan LCQ-Duo using the Xcalibur (Finnigan, San Jose, CA) software package and the electrospray source. The solutions utilized were the same as those previously described, diluted by a factor of ten. The pressure was maintained at nominally 5×10^{-6} torr with helium in the absence of ESI. For ESI experiments, the sample flow rate was 3 μL/min, and the pressure in the analyzer region was then nominally 1×10^{-5} torr with helium buffer gas. Ionization and trapping conditions were optimized for each of the macrolides; re-tuning for individual samples was seldom necessary.

Erythromycin A and B and oleandomycin were obtained from Sigma Chemical (St. Louis, MO). SP1 and SP2 were degraded from natural erythromycin B [31]. SP3 [32] and SP4 [33] were prepared by synthetic methods.

Results and Discussion

Protonated Macrolides and Analogs

For simplicity in discussing the four synthetic precursors, each is assigned an abbreviated designation: Synthetic precursor (SP1–4), as shown in Figure 1. Examples of the CAD and IRMPD spectra for two of the protonated macrolides are shown in Figures 2 and 3 for erythromycin A and SP3. The CAD data was obtained by using the commercial LCQ instrument, whereas the IRMPD data was obtained with the home-built ion trap instrument because it was felt that the CAD data from the LCQ instrument would be more useful to the growing number of users of commercial ion trap instruments. Thus, in this report the best CAD data (from the LCQ ion trap) is compared to the best IRMPD data available (from the home-built instrument). Both CAD and IRMPD data for all seven protonated compounds are summarized in Table 1. The most prevalent fragmentation pathways include dehydration (for four of the macrolides) and loss of the cladinose sugar (for the four that possess the cladinose moiety) (Scheme **1**). In the IRMPD spectra, the formation of a characteristic desosamine ion at *m/z* 158 for protonated erythromycin A and B, SP1, SP2, and SP3 is also significant (Scheme **1**). This fragment ion is not observed in the analogous CAD spectra because the mass is too low to be trapped efficiently under the conditions needed for activation of the high mass precursors. The schemes presented in this work offer proposed fragment ion structures that are consistent with genealogical pathways and secondary fragmentation information obtained from multi-stage IRMPD (MS^n) experiments, as discussed later.

The IRMPD and CAD spectra of protonated erythromycin A have comparable signal intensities, dissociation efficiencies, and fragment ions (Figure 2), with the notable exception of the absence of the characteristic desosamine ion at *m/z* 158 in the CAD spectrum. Both spectra show two water losses, loss of the cladinose sugar (−158 aμ, formation of *m/z* 576), and further water losses from the macrolide ring. Protonated erythromycin B displays one less loss of water than erythromycin A in both the IRMPD and CAD spectra (Figure 4), implying that the C-12 hydroxyl accounts for this extra step of dehydration in protonated erythromycin A. Protonated oleandomycin dissociates by the loss of the hexapyranose moiety in both the IRMPD and CAD spectra (formation of *m/z* 544), loss of both sugars (formation of *m/z* 387), and by formation of the desosamine ion (*m/z* 158) (IRMPD only). The absence of dehydration, a loss that was significant for both protonated erythromycin A and B, is accounted for by the lack of a hydroxyl group at C-6 [5]. Apparently the C-11 hydroxyl group is not a viable route for dehydration in these macrolides.

Protonated SP1 (with a C-9 hydroxyl instead of a carbonyl) and SP4 (in which the C-9 oxygen is involved in binding to the trimethylbenzyl protecting group) exhibit virtually no water loss in either the CAD or IRMPD spectra, corroborating the C-6/C-9 oxonium formation mechanism proposed by Gates et al. [4], in which the carbonyl oxygen at C-9 was involved in dehydration. The dissociation spectrum of protonated SP3 displays a small signal corresponding to water loss; the presence of a new hydroxyl group at C-3 likely accounts for this fragmentation pathway. Protonated

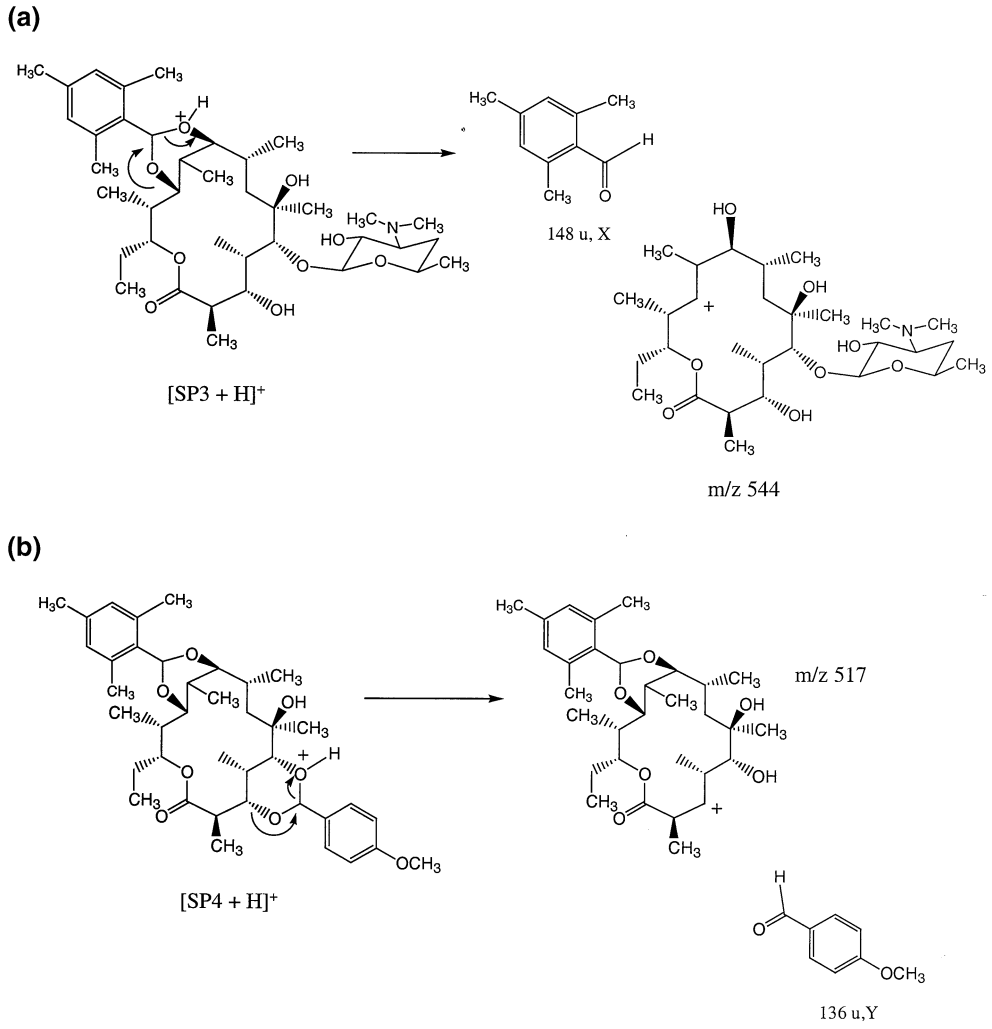

Scheme 2

SP2 undergoes extensive dehydration, thus confirming that the presence of the C-3 hydroxyl group promotes dehydration even in the absence of the C-9 carbonyl. Loss of desosamine as a neutral is a significant pathway only for protonated SP3, the only compound lacking the less basic cladinose moiety and in which the C-9 and C-11 oxygens bridge a trimethylbenzyl substituent, thus suppressing the typical dehydration pathway.

SP3 and SP4 are interesting cases because both lack the cladinose sugar, and the active C-9 oxygen (which is key for the dominant dehydration step in the other macrolides) is bound to a trimethylbenzyl substituent. In addition, SP4 lacks the desosamine moiety, and the C-5 and C-3 oxygens are bound to a p-methoxybenzyl substituent. For protonated SP3, the loss of the trimethylbenzyl substituent is a dominant pathway, despite the fact that this substituent is connected to the macrolide ring by two carbon–oxygen bonds. One route that accounts for this loss is shown in Scheme **2a**, but the site of the ionizing proton has not been confirmed. For protonated SP4, the elimination of the trimethylbenzyl substituent is not observed; instead, the loss of the other substituent is dominant (Scheme **2b**).

Other than the notable absence of the lower mass fragment ions in the CAD spectra that are prominent in the IRMPD spectra, the CAD and IRMPD spectra are qualitatively similar. In both the IRMPD and CAD spectra, cleavages of the macrolide ring are absent or insignificant. Moreover, neither IRMPD nor CAD provide sufficient diagnostic fragment ions to confirm the protecting groups at each position of SP4. These latter two shortcomings prompted our interest in lithium cationization as an alternative to protonation to produce precursor ions that potentially would give complementary structural information upon activation.

Lithium Cationized Macrolides

Production of lithium-cationized complexes only required the addition of a lithium salt to the solutions containing the macrolides, so it is an easy way to create ions that may give complementary or more diagnostic

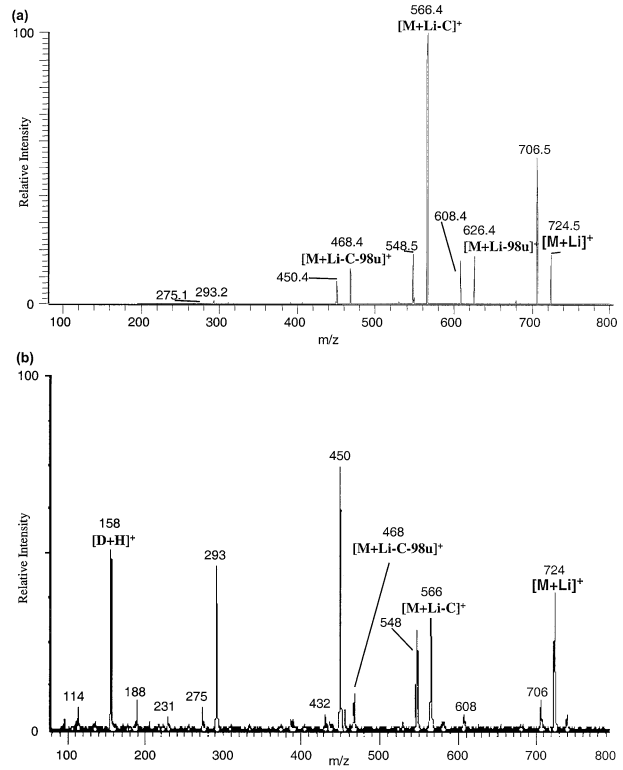

Figure 5. (**a**) CAD and (**b**) IRMPD of lithium-cationized erythromycin B.

structural information compared to that obtained for protonated molecules. While overall signal intensities were of the same order of magnitude for either ionization technique, the alkali metal complexes tended to produce more fragments than the protonated counterparts upon CAD or IRMPD. Examples of the fragmentation patterns obtained for the lithium-cationized species are shown for erythromycin B (Figure 5) and SP4 (Figure 6), and all of the IRMPD and CAD data is summarized in Table 2.

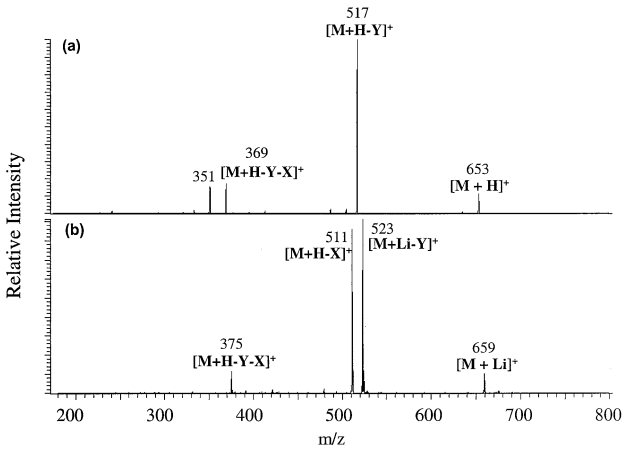

Figure 6. CAD of (**a**) protonated and (**b**) lithium-cationized SP4.

There are three notable changes in the dissociation pattern of lithium-cationized erythromycin A compared to that of protonated erythromycin A. First, dehydration is generally limited to a single water loss instead of the two or three seen for protonated erythromycin A. In addition, two new diagnostic fragment ions are observed for lithium-cationized erythromycin A, one at *m/z* 626 and one at *m/z* 608. A pathway rationalizing the loss of 114 u is shown in Scheme **3**, and clearly cleavages of the macrolide ring are required for this fragmentation pathway, a type of process notably absent for the protonated species. Presumably this type of process also accounts for the loss of 132 u, which requires the loss of one water molecule in conjunction with the loss of 114 u. Cleavages of the macrolide ring were not observed for the protonated species, suggesting that the lithium cationization process substantially changes the activation/dissociation processes of the macrolides. The macrolide cleavage pathways are somewhat more significant for lithium-cationized erythromycin B and oleandomycin in which the losses of 98 u or 116 u for erythromycin B and loss of 84 u for oleandomycin are analogous to those observed for erythromycin A. The mass shifts in these neutral losses compared to those observed for lithium-cationized erythromycin A are accounted for by the absence of the C-12 hydroxyl group in erythromycin B (difference of 16 u) and the lack of the C-12 hydroxy group and C-13 methylene group in oleandomycin (difference of 30 u). The loss of 84 u does not occur in conjunction with dehydration for lithium-cationized oleandomycin presumably because of the absence of the C-6 hydroxyl group, as noted earlier for the dissociation of protonated oleandomycin. For lithium-cationized erythromycin A and B, additional new fragment ions at *m/z* 450 and 468 indicate that the macrolide ring cleavage illustrated in Scheme **3** may also occur in conjunction with the standard loss of the cladinose ring. In fact, for both lithium-cationized erythromycin A and B, a new fragment ion at *m/z* 293 appears, attributed to loss of desosamine (157 u) in combination with the loss of the cladinose moiety and the diagnostic macrolide ring cleavage. (This fragment ion is only significant in the IRMPD spectra.) This combination of neutral losses is supported by multistage IRMPD (MS^n) experiments. For lithium-cationized oleandomycin, the loss of 84 u may occur in conjunction with the loss of the hexapyranose moiety. A new fragmentation pathway that emerges for lithium-cationized oleandomycin is the loss of formaldehyde, a process that apparently involves the epoxide moiety at the C-8 position. This simple loss, not observed for protonated oleandomycin, provides a key way to confirm the epoxide substituent.

Both protonated and lithium-cationized SP1 give one major fragment, loss of cladinose. Of all the macrolides analyzed, SP1 shows the fewest differences in the fragmentation patterns of the protonated and lithium-cationized species. Two new fragment ions that emerge for the lithium-cationized species are the loss of cladi-

Table 2. CAD and IRMPD data for lithium-cationized macrolides

Compound	Parent (*m/z*)	Fragment (*m/z*)	Neutral loss	CAD Results Percent	IRMPD Results Percent
Erythromycin A	740	722	18	37%	7%
		626	114	2%	—
		608	132	2%	—
		582	158	44%	16%
		564	176	13%	37%
		546	194	<1%	5%
		468	272	1%	—
		450	290	1%	13%
		293	447	<1%	12%
		158	582	—	10%
Erythromycin B	724	706	18	23%	3%
		706	18	23%	3%
		626	98	8%	—
		608	116	7%	2%
		566	158	44%	12%
		548	176	8%	10%
		468	256	6%	4%
		450	274	4%	27%
		293	431	<1%	17%
		275	449	<1%	3%
		158	566	—	19%
		116	610	—	3%
Oleandomycin	694	664	30	13%	1%
		610	84	7%	1%
		550	144	69%	27
		537	157	2%	3%
		532	162	3%	1%
		466	228	4%	5%
		393	301	1%	1%
		375	319	1%	1%
		309	385	—	1%
		158	536	—	55%
		116	578	—	4%
SP1	726	568	158	96%	58%
		506	220	2%	3%
		440	286	<1%	2%
		411	315	2%	4%
		176	550	—	1%
		158	568	—	26%
		116	612	—	6%
SP2	568	550	18	5%	No Data
		523	45	3	
		506	62	33%	
		498	70	3	
		494	74	4%	
		453	115	3%	
		440	128	8%	
		411	157	31%	
		393	175	8%	
		377	193	2%	
SP3	698	680	18	22%	No Data
		636	62	12%	
		624	74	4%	
		582	116	3%	
		550	148	27%	
		541	157	6%	
		530	168	7%	

(continued)

Table 2. Continued

Compound	Parent (*m/z*)	Fragment (*m/z*)	Neutral loss	CAD Results Percent	IRMPD Results Percent
		523	175	14%	
		450	248	2%	
		393	305	3%	
SP4	659	641	18	<1%	1%
		523	136	45%	16%
		511	148	44%	22%
		479	180	4%	2%
		375	284	5%	11%
		293	366	1%	8%
		277	382	<1%	10%
		118	541	—	23%
		106	553	—	7%

nose in conjunction with either the loss of 62 u, giving a product at *m/z* 506, or the loss of 128 u, giving a fragment ion at *m/z* 440. These eliminations of 62 or 128 u are highly diagnostic losses discussed later for lithium-cationized SP2 and SP3, thus representing very characteristic fragmentation pathways for these three macrolides.

The fragmentation pattern of lithium-cationized SP2 is much richer than that of the protonated species, which predominantly lost water and/or desosamine. Three new fragmentation pathways are the losses of 62 u, 70 u, or 128 u, which may occur consecutively based on MS^n experiments and involve cleavages of the macrolide ring. Proposed fragments to account for these losses are illustrated in Scheme **4**. The specific site of dehydration is not known. In addition to the same fragmentation processes seen for protonated SP3 (i.e., dehydration, loss of desosamine, loss of the trimethyl benzyl group), lithium cationized SP3 also dissociates by loss of the characteristic 62 u species.

The effect of lithium cationization on the dissociation of SP4 is especially striking, as illustrated by the CAD spectra shown in Figure 6. In addition to the dominant loss of 136 u (the trimethyl benzyl substituent, formation of *m/z* 523) that was observed upon dissociation of protonated SP4, the loss of the other substituent, the p-methoxybenzyl group (loss of 148 u, formation of *m/z* 511), is also evident. These losses are depicted in Scheme **5**. In the lithium-containing products shown in Scheme **5**, further hydrogen migrations may occur to allow favorable delocalization of the charge and multisite coordination of lithium. The ability to lose either substituent likely relates to the greater delocalization of the lithium ion compared to that of an ionizing proton in the macrolide.

As noted above in the comparison of the IRMPD and

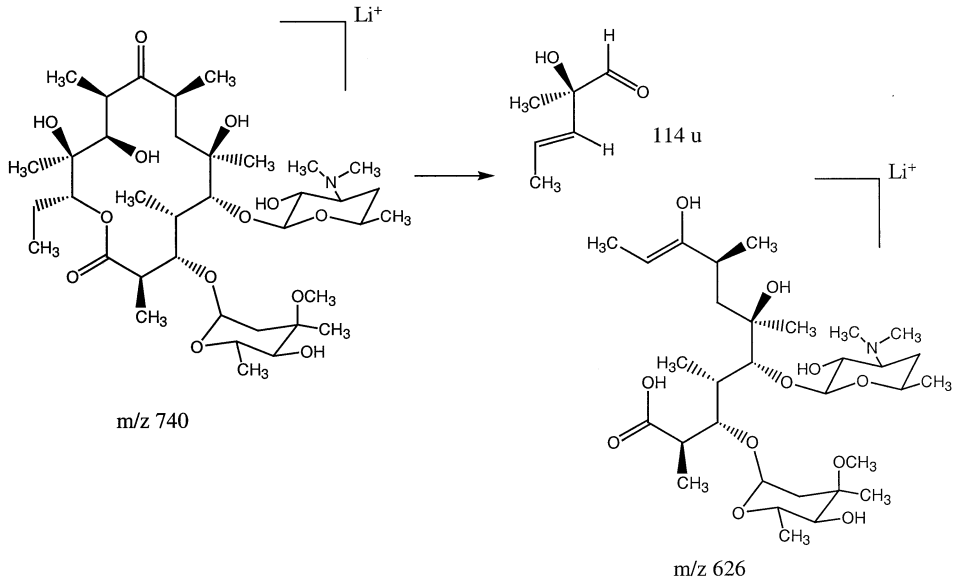

Scheme 3

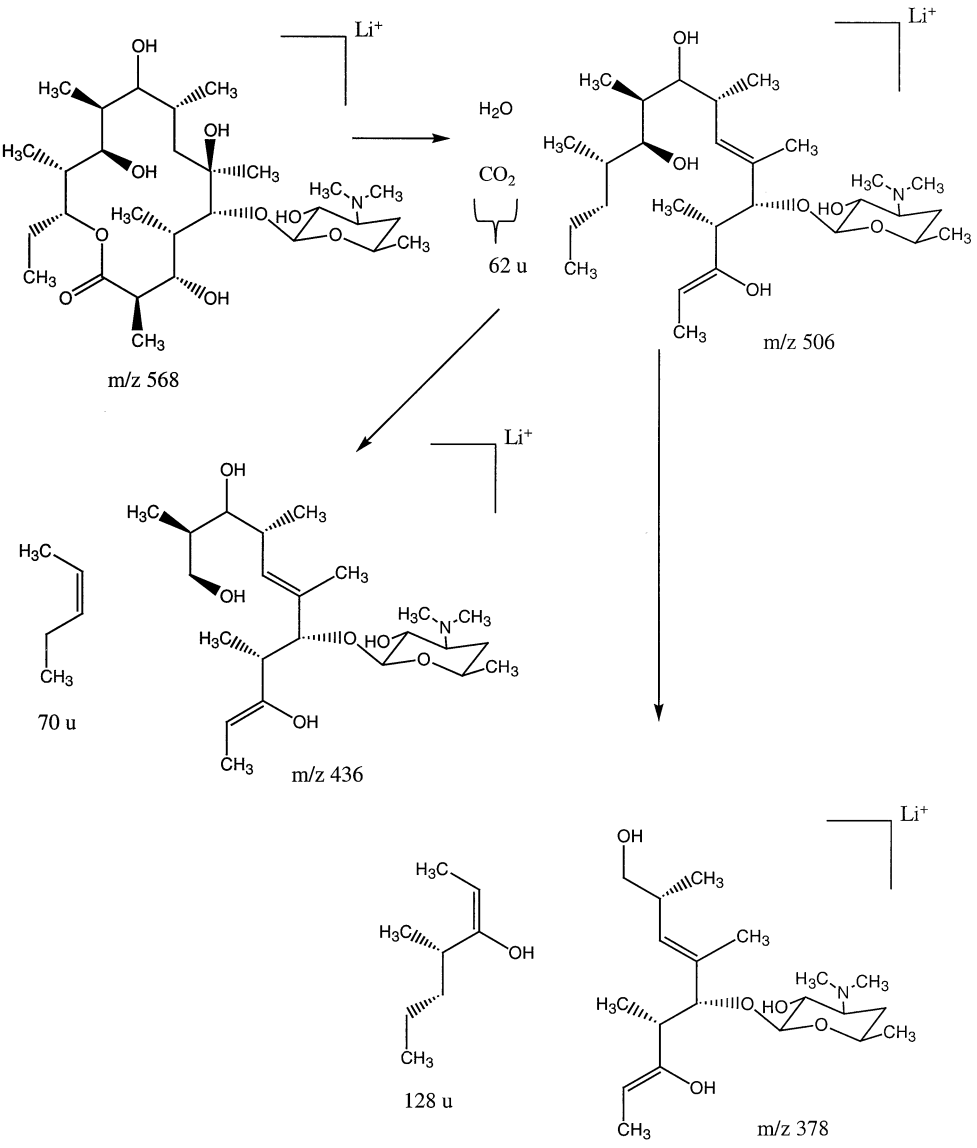

Scheme 4

CAD spectra for the protonated macrolides, the IRMPD spectra for the lithium-cationized compounds also show more intense mid- and lower mass fragment ions, presumably due to the ability to effectively trap these ions because the lower mass storage range is not cut off as in the CAD experiments. Interestingly, the formation of the desosamine ion at *m/z* 158 (refer to Scheme **1** for the proposed structure of this ion) is still observed in the IRMPD spectra for the lithium-cationized compounds. IRMPD of lithium-cationized SP2 and SP3 was unsuccessful because of the inadequate ion isolation capability of the in-house IRMPD/ion trap system, a problem that potentially will be corrected by the use of a more advanced arbitrary waveform generator. The poor isolation is not attributed to the IRMPD experiment itself because isolation was similarly poor when attempting CAD experiments for SP2 and SP3.

Time-Variable IRMPD and Multi-Stage IRMPD (MS^n)

One way to extend the diagnostic utility of the IRMPD method is to monitor the IRMPD spectra as a function of the irradiation time. The resulting time-resolved data allow selection of the IRMPD conditions for optimization of the fragmentation patterns and give an initial assessment of potential genealogical relationships of the fragment ions. An example of the time-resolved data obtained for one of the protonated macrolides, SP1, is shown in Figure 7. The dominant fragment ion at low activation times is *m/z* 562, resulting from the loss of the cladinose substituent. As the irradiation time increases, these primary fragment ions absorb sufficient photons to dissociate, thus causing a reduction in the intensity of the *m/z* 562 ion and production of *m/z* 158, the des-

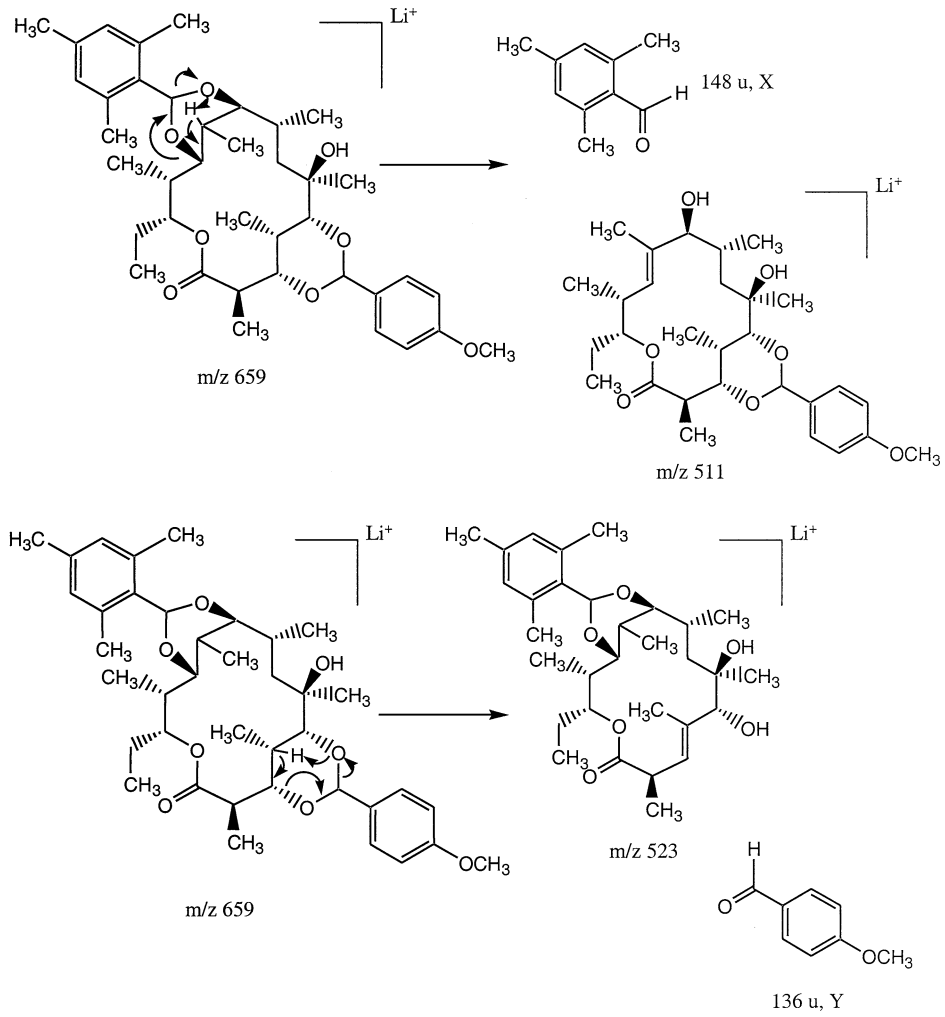

Scheme 5

osamine ion. This behavior implies both a genealogical relationship and allows an effective way to tune the IRMPD conditions to optimize the formation of specific fragments for further interrogation.

Discrete stages of isolation and activation give more specific genealogical information than that obtained by time-variable IRMPD or energy-variable CAD. Multi-stage IRMPD (MS^n) is particularly efficient because the losses due to ion scattering that may occur with multiple stages of CAD are virtually eliminated. An example

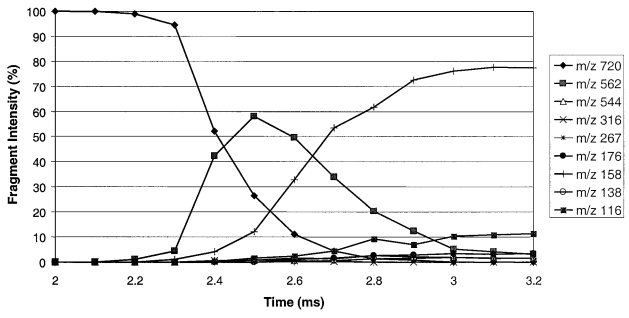

Figure 7. Time-variable IRMPD of protonated SP1.

of the utility of multi-stage IRMPD is shown in Figure 8 for protonated erythromycin B. The IRMPD spectrum is shown in Figure 8a, and the major fragments are due to dehydration (*m/z* 700) or loss of cladinose (*m/z* 560), or loss of cladinose and one or two units of water (*m/z* 542 and 524). In formulating mechanisms to account for these pathways and to develop predictions for related analogs, it would be useful to know whether the macrolide dehydrates prior to or after the loss of cladinose and whether all of the primary fragments dissociate further to produce the desosamine ion at *m/z* 158. In Figure 8b, the IRMPD spectrum obtained for the dehydrated macrolide is shown. It dissociates by loss of the cladinose ring, a second water loss, and formation of the desosamine ion at *m/z* 158. Figure 8c shows that isolation and activation of *m/z* 560, the primary fragment resulting from loss of cladinose from the protonated macrolide, results in dehydration or formation of *m/z* 158. Isolation of the secondary fragment ion, *m/z* 542, indicates that this ion does not dehydrate but instead dissociates to form the desosamine ion. This sequence of IRMPD experiments indicates that all of the primary fragments ultimately may result in the des-

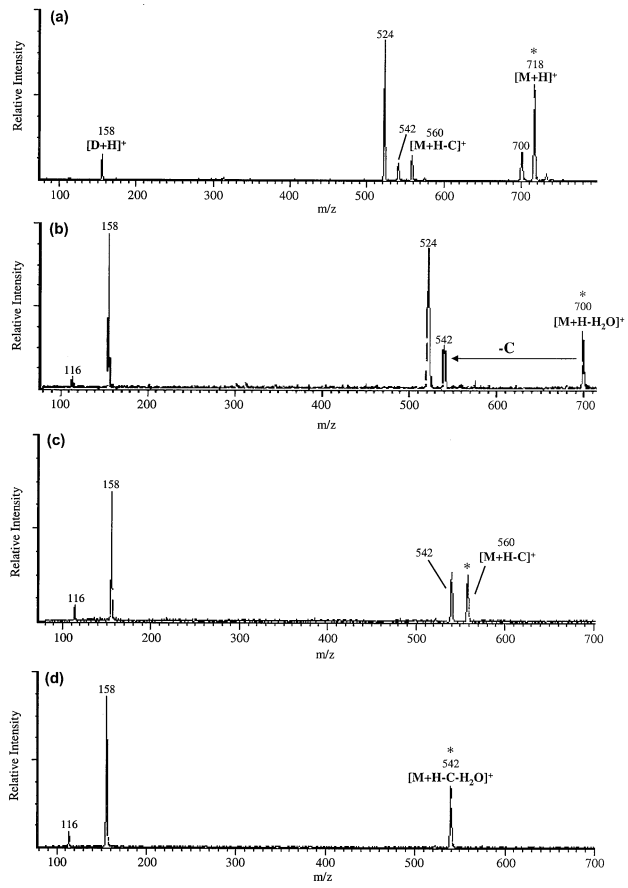

Figure 8. IRMPD mass spectra of protonated erythromycin B. (**a**) IRMPD of protonated erythromycin B. (**b**) IRMPD/IRMPD of the fragment ion at *m/z* 700 from protonated erythromycin B. (**c**) IRMPD/IRMPD of the fragment ion at *m/z* 560 from protonated erythromycin B. (**d**) IRMPD/IRMPD/IRMPD of the fragment ion at *m/z* 542 from *m/z* 560 from protonated erythromycin B.

osamine ion, that dehydration and loss of cladinose may occur in either order, but that if the protonated macrolide loses the cladinose moiety, it may not undergo two stages of dehydration. The multi-stage IRMPD spectral results are summarized in Table 3.

For protonated erythromycin A, a second stage of IRMPD on the fragment ion at *m/z* 576 (due to loss of cladinose) formed upon IRMPD of the protonated macrolide indicates that this fragment ion may undergo up to three steps of dehydration, whereas protonated erythromycin A undergoes only two steps of dehydration. This additional step of dehydration for the *m/z* 576 fragment suggests that the hydroxyl group at the C-3 position (see Scheme **1**), involved in a glycosidic bond for protonated erythromycin A, may be key for this process. The multi-stage IRMPD spectra for the fragment ion at *m/z* 158 is identical for both protonated erythromycin A and B.

The IRMPD spectrum of the *m/z* 562 fragment from protonated SP1 gives the same dominant fragment ions that are observed for protonated SP1. This suggests that many of the lower mass fragment ions may occur through consecutive dissociation steps after loss of the cladinose sugar. For protonated SP2, a similar behavior is observed, in which IRMPD of *m/z* 544, formed upon dehydration of protonated SP2, gives the same four most dominant fragment ions as observed for IRMPD of protonated SP2. These four ions, *m/z* 176, 158, 138, and 116, are all characteristic of the desosamine moiety. Protonated SP3 produced *m/z* 544 (loss of the trimethyl benzyl substituent) as the second most dominant fragment ion upon IRMPD. IRMPD of this primary fragment ion again resulted in the ions diagnostic for the desosamine moiety. Upon activation protonated SP4 dissociated by loss of the methoxybenzyl substituent (136 u) as one of the major characteristic pathways. Isolation and IRMPD of this fragment ion (*m/z* 517) predominantly results in the loss of the other substituent, the trimethyl benzyl moiety (148 u), which may occur in conjunction with dehydration.

Multi-stage IRMPD experiments are particularly useful for probing the fragmentation pathways of the lithium-cationized compounds in greater detail because more extensive cleavages of the macrolide ring are involved rather than just simple losses of the substituents or sugars. For example, two of the macrolide ring cleavages that were observed upon IRMPD of lithium-cationized erythromycin A were loss of 114 u (proposed in Scheme **3**) or loss of 132 u (presumably loss of 114 u in conjunction with dehydration). IRMPD allows further confirmation of these pathways, as summarized in Table 3. A second stage of IRMPD on *m/z* 582 (loss of cladinose) results in the loss of 132 u (formation of *m/z* 450) or loss of water (formation of *m/z* 564). IRMPD of *m/z* 450 results in the loss of the desosamine moiety as the dominant fragment ion (formation of *m/z* 293). A third stage of IRMPD on *m/z* 293 yields the diagnostic loss of 62 u seen for many of the other lithium-cationized compounds (i.e., Scheme **4**). This series of IRMPD experiments indicates that the loss of water that occurs in conjunction with the diagnostic macrolide cleavage (loss of 114 u) may occur either before or after the loss of 114 u, and likewise the loss of 114 u may occur before or after the loss of the cladinose moiety. For lithium-cationized erythromycin B, a similar genealogical pattern is observed, with the diagnostic macrolide ring cleavage (loss of 98 u) occurring before or after dehydration and before or after the loss of cladinose. Multi-stage IRMPD confirms the genealogical relationships illustrated in Scheme **4** for lithium-cationized SP1 and SP2, in which activation of *m/z* 506 produces fragment ions at both *m/z* 436 and 378. Loss of the desosamine moiety (157 u) is also possible from *m/z* 506. Multi-stage IRMPD of lithium-cationized SP4 confirms that loss of either the trimethyl benzene or methoxybenzene substituent may occur first. In general, the multi-stage IRMPD spectra provide more specific fragmentation information than just a single stage of IRMPD, giving greater diagnostic identification of the macrolides when present in mixtures and allowing construction of self-consistent fragmentation pathways.

Table 3. Multi-step IRMPD results

Protonated compounds Compound	IRMPD step	Parent (*m/z*) or sequence	Fragment (*m/z*)	Neutral loss	Percent
Erythromycin A	1[a]	734	716	18	6%
			698	36	6%
			576	158	21%
			558	176	6%
			540	194	6%
			522	212	10%
			316	418	2%
			158	576	40%
			116	618	3%
	2	734 → 576 →	558	18	6%
			540	36	7%
			522	54	7%
			158	418	72%
			116	460	8%
	3	734 → 576 → 158	116	42	25%
			114	44	24%
			98	60	12%
			83	75	39%
Erythromycin B	1	718	700	18	12%
			560	158	11%
			542	176	8%
			524	194	57%
			316	402	1%
			158	560	10%
			116	602	1%
	2	718 → 700 →	542	158	13%
			524	176	40%
			158	542	43%
			116	584	4%
	2	718 → 560 →	542	18	26%
			158	402	65%
			116	444	9%
	3	718 → 718 → 524 →	302	222	9%
			148	366	84%
			116	408	7%
	3	718 → 560 → 542	158	384	90%
			116	426	10%
	3	718 → 560 → 158	116	42	22%
			98	60	20%
			83	75	19%
Oleandomycin	1	688	544	144	42%
			302	386	1%
			158	530	54%
			116	572	3%
	2	688 → 544	158	386	96%
			116	428	4%
SP1	1	720	562	158	42%
			544	176	2%
			316	404	1%
			176	544	2%
			158	562	49%
			116	604	4%

(continued)

Table 3. Continued

Protonated compounds Compound	IRMPD step	Parent (*m/z*) or sequence	Fragment (*m/z*)	Neutral loss	Percent
	2	720 → 562 →	544	18	3%
			405	157	1%
			387	175	<1%
			369	193	<1%
			351	211	1%
			267	295	2%
			176	386	3%
			158	404	78%
			138	424	2%
			116	446	10%
SP2	1	562	544	18	3%
			387	175	1%
			351	211	2%
			267	295	2%
			176	386	3%
			158	404	75%
			138	424	2%
	2	562 → 544 →	176	368	10%
			158	386	58%
			138	406	11%
			116	428	21%
	3	562 → 544 → 176 →	158	18	89%
			116	60	11%
SP3	1	692	674	18	1%
			544	148	24%
			535	157	1%
			526	166	2%
			517	175	<1%
			387	305	2%
			369	323	1%
			351	341	2%
			267	425	2%
			176	516	6%
			158	534	53%
			138	554	3%
			116	576	4%
	2	692 → 544 →	176	368	30%
			158	386	49%
			138	406	14%
			116	428	7%
SP4	1	653	635	18	1%
			517	136	13%
			505	148	1%
			487	166	4%
			369	284	13%
			351	302	29%
			333	320	9%
			266	387	5%
			241	412	7%
			227	426	9%
			120	533	9%
	2	653 → 517 →	369	148	34%
			351	166	32%

(continued)

Table 3. Continued

Protonated compounds Compound	IRMPD step	Parent (*m/z*) or sequence	Fragment (*m/z*)	Neutral loss	Percent
			241	276	15%
			227	290	19%
Lithiated compounds					
Compound	IRMPD step	Parent (*m/z*) or sequence	Fragment (*m/z*)	Neutral loss	Percent
Erythromycin A	1	740	722	18	7%
			582	158	16%
			564	176	37%
			546	194	5%
			450	290	13%
			293	447	12%
			158	582	10%
	2	740 → 582 →	564	18	55%
			450	132	25%
			407	175	12%
			394	188	8%
	2	740 → 564 →	546	18	3%
			450	114	12%
			407	157	4%
			389	175	4%
			293	271	14%
			275	289	7%
			231	333	12%
			223	341	23%
			191	373	14%
			158	406	7%
	2	740 → 450 →	407	43	22%
			293	157	78%
	3	740 → 564 → 293 →	275	18	12%
			231	62	15%
			191	102	38%
			179	114	10%
			173	120	12%
			161	132	13%
Erythromycin B	1	724	706	18	3%
			608	116	2%
			566	158	12%
			548	176	10%
			468	256	4%
			450	274	27%
			293	431	17%
			275	449	3%
			158	566	19%
			116	610	3%
	2	724 → 566 →	548	18	14%
			468	98	5%
			450	116	39%
			409	157	2%
			391	175	4%
			293	273	24%
			275	291	6%
			231	335	6%
	2	724 → 548 →	468	80	2%
			450	98	31%

(continued)

Table 3. Continued

Protonated compounds Compound	IRMPD step	Parent (*m/z*) or sequence	Fragment (*m/z*)	Neutral loss	Percent
			432	116	3%
			409	139	2%
			391	157	4%
			293	255	26%
			275	273	7%
			231	317	8%
			188	360	13%
			158	408	6%
	2	724 → 450 →	409	41	2%
			391	59	2%
			321	129	4%
			293	157	36%
			275	175	9%
			231	219	15%
			191	259	19%
			158	292	13%
	3	724 → 548 → 293 →	275	18	8%
			249	44	5%
			231	62	29%
			219	74	6%
			191	102	52%
Oleandomycin	1	694	664	30	1%
			610	84	1%
			550	144	27%
			537	157	3%
			532	162	1%
			466	228	5%
			393	301	1%
			375	319	1%
			309	385	1%
			158	536	55%
			116	578	4%
	2	694 → 550 →	520	30	2%
			466	84	17%
			393	157	4%
			375	175	3%
			309	241	14%
			291	259	5%
			217	333	6%
			158	392	37%
			138	412	4%
			116	434	8%
	2	694 → 466 →	404	62	4%
			392	74	3%
			351	115	3%
			309	157	31%
			291	175	13%
			263	203	10%
			235	231	10%
			229	237	8%
			217	249	12%
			158	308	6%
	3	694 → 466 → 309 →	291	18	13%
			263	46	19%
			247	62	10%

(continued)

Table 3. Continued

Protonated compounds Compound	IRMPD step	Parent (*m/z*) or sequence	Fragment (*m/z*)	Neutral loss	Percent
			235	74	10%
			201	108	30%
			173	136	18%
SP1	1	726	568	158	58%
			506	220	3%
			440	286	2%
			411	315	4%
			176	550	1%
			158	568	26%
			116	612	6%
	2	726 → 568 →	550	18	2%
			506	62	13%
			440	128	7%
			422	146	5%
			411	157	21%
			393	175	10%
			375	193	18%
			349	219	6%
			283	285	7%
			265	303	11%
	3	726 → 568 → 506 →	436	70	7%
			378	128	68%
			349	157	8%
			203	303	17%
	3	726 → 568 → 440 →	422	18	15%
			378	62	26%
			265	175	14%
			221	219	10%
			203	237	21%
			163	277	14%
	3	726 → 568 → 411 →	393	18	10%
			349	62	9%
			283	128	17%
			265	146	21%
			221	190	19%
			203	208	12%
			163	248	12%
	3	726 → 568 → 393 →	375	18	12%
			295	98	8%
			265	128	17%
			221	172	8%
			203	190	18%
			193	200	16%
			179	214	13%
			163	230	8%
	3	726 → 568 → 375 →	357	18	3%
			305	70	5%
			221	154	10%
			203	172	36%
			179	196	21%
			163	212	25%
SP4	1	659	641	18	1%
			523	136	16%

(continued)

Table 3. Continued

Protonated compounds Compound	IRMPD step	Parent (*m/z*) or sequence	Fragment (*m/z*)	Neutral loss	Percent
			511	148	22%
			479	180	2%
			375	284	11%
			293	366	8%
			275	382	10%
			118	541	23%
			106	553	7%
	2	659 → 523 →	375	148	4%
			293	230	16%
			231	292	20%
			189	334	16%
			128	395	15%
			118	405	15%
			106	417	14%
	2	659 → 511 →	413	98	6%
			375	136	6%
			348	163	6%
			293	218	4%
			275	235	14%
			231	280	7%
			212	299	8%
			204	307	8%
			118	393	27%
			106	405	14%

Conclusions

Three main conclusions are derived from the present comparison of IRMPD and CAD for structural characterization of protonated and lithium-cationized macrolides. First, the IRMPD spectra contain key diagnostic fragment ions, especially the desosamine ion, not observed in the CAD spectra because of the trapping limitations that occur when higher mass ions are resonantly activated in the ion trap and/or lack of formation of these ions under CAD conditions. Second, multistage IRMPD proves particularly useful for confirming the genealogical relationships of dissociation, especially when low mass fragment ions that are not effectively stored under CAD conditions are formed, which ultimately gives support to the proposed fragmentation pathways and fragment ion structures. Third, the lithium-cationization process results in more extensive and more diagnostic fragmentation than that observed for the protonated macrolides. In particular, mapping of the substituents for the synthetic precursors is possible for the lithium-cationized complexes because the losses of the substituents are observed directly upon IRMPD or CAD. Moreover, characteristic cleavages of the macrolide rings are evident for the lithium-cationized complexes.

Acknowledgments

JSB acknowledges support from the National Science Foundation (CHE-9820755) and the Robert A. Welch Foundation (grant no. F1155). The authors gratefully acknowledge Dr. Stephen F. Martin for generously supplying synthetic intermediates of erythromycin used in this study. Dr. Stephen F. Martin acknowledges support from the Robert A. Welch Foundation and the National Institutes of Health.

References

1. (a) Khosla, C. Harnessing the Biosynthetic Potential of Modular Polyketide Synthases. *Chem. Rev.* **1997,** *97,* 2577–2590. (b) Staunton, J.; Wilkinson, B. Biosynthesis of Erythromycin and Rapamycin. *Chem. Rev.* **1997,** *97,* 2611–2629.
2. Kirst, H. A. Structural Modification of Macrolide Antibiotics. *In Recent Progress in the Chiral Synthesis of Antibiotics;* Lukacs, G.; Ohno, M., Eds.; Springer-Verlag: Berlin, 1990; 39–63.
3. Cerny, R. L.; MacMillan, D. K.; Gross, M. L.; Mallams, A. K.; Pramanik, B. N. Fast-Atom Bombardment and Tandem Mass Spectrometry of Macrolide Antibiotics. *J. Am. Soc. Mass Spectrom.* **1994,** *5,* 151–158.
4. Gates, P. J.; Kearney, G. C.; Jones, R.; Leadlay, P. F.; Staunton, J. Structural Elucidation of Erythromycins by Electrospray Tandem Mass Spectrometry. *Rapid Commun. Mass Spectrom.* **1999,** *13,* 242–246.
5. Kearney, G. C.; Gates, P. J.; Leadlay, P. F.; Staunton, J.; Jones, R. Structural Elucidation Studies of Erythromycins by Electrospray Tandem Mass Spectrometry II. *Rapid Commun. Mass Spectrom.* **1999,** *13,* 1650–1656.
6. Volmer, D. A.; Hui, J. P. M. Study of Erythromycin A Decomposition Products in Aqueous Solution by Solid-Phase Microextraction/Liquid Chromatography/Tandem Mass Spectrometry. *Rapid Commun. Mass Spectrom.* **1998,** *12,* 123–129.
7. Delepine, B.; Hurtaud-Pessel, D.; Sanders, P. Multiresidue Method for Confirmation of Macrolide Antibiotics in Bovine

Muscle by Liquid Chromatography/Mass Spectrometry. *J. AOAC Int.* **1996,** *79,* 397–404.
8. Hirsch, R.; Ternes, T. A.; Haberer, K.; Mehlich, A.; Ballwanz, F.; Kratz, K.-L. Determination of Antibiotics in Different Water Compartments via Liquid Chromatography/Electrospray Tandem Mass Spectrometry. *J. Chromatog. A* **1998,** *815,* 213–223.
9. Ling, Y.-C.; Lin, L.; Chen, Y.-T. Quantitative Analysis of Antibiotics by Matrix-Assisted Laser Desorption/Ionization Time-of-Flight Mass Spectrometry. *Rapid. Comm Mass Spectrom.* **1998,** *12,* 317–327.
10. Asam, M. R.; Glish, G. L. Tandem Mass Spectrometry of Alkali Cationized Polysaccharides in a Quadrupole Ion Trap. *J. Am. Soc. Mass Spectrom.* **1997,** *8,* 987–995.
11. Hsu, F.-F.; Bohrer, A.; Turk, J. Formation of Lithiated Adducts of Glycerophosphocholine Lipids Facilitates their Identification by Electrospray Ionization Tandem Mass Spectrometry. *J. Am. Soc. Mass Spectrom.* **1998,** *9,* 516–526.
12. Olling, A.; Breimer, M. E.; Peltomaa, E.; Samuelsson, B. E.; Ghardashkhani, S. Electrospray Ionization and Collision-Induced Dissociation Time-of-Flight Mass Spectrometry of Neutral Glycosphingolipids. *Rapid Commun. Mass Spectrom.* **1998,** *12,* 637–645.
13. Madhusudanan, K. P.; Raj, K.; Bhaduri, A. P. Effect of Metal Cationization on the Low-Energy Collision-Induced Dissociation of Loganin, Epi-Loganin, and Keologanin Studied by Electrospray Ionization Tandem Mass Spectrometry. *J. Mass Spectrom.* **2000,** *25,* 901–911.
14. Stone, J. A.; Vukomanovic, D. Electrospray and Collisionally Activated Dissociation Study of the Association of Pyocyanin with Alkali Metal Cations and Doubly Charged Alkaline Earth and Zinc Cations. *Int. J. Mass Spectrom.* **2001,** *210/211,* 341–359.
15. Cui, M.; Song, F.; Liu, Z.; Liu, S. Metal Ion Adducts in the Structural Analysis of Ginsenosides by Electrospray Ionization with Multi-Stage Mass Spectrometry. *Rapid Commun. Mass Spectrom.* **2001,** *15,* 586–595.
16. Stephenson, J. L., Jr.; Booth, M. M.; Boue, S. M.; Eyler, J. R.; Yost, R. A. Analysis of Biomolecules Using Electrospray Ionization-Ion Trap Mass Spectrometry and Laser Photodissociation. *In Biochemical and Biotechnological Applications of Electrospray Ionization Mass Spectrometry;* Snyder, A. P., Ed.; Am. Chem. Soc.: Washington, D.C., 1996; 601.
17. Colorado, A.; Shen, J. X.; Vartanian, V. H.; Brodbelt, J. Use of Infrared Multiphoton Dissociation with SWIFT for Electrospray Ionization and Laser Desorption Applications in a Quadrupole Ion Trap Mass Spectrometer. *Anal. Chem.* **1996,** *68,* 4033–4043.
18. Little, D. P.; Speir, J. P.; Senko, M. W.; O'Connor, P. B.; McLafferty, F. W. Infrared Multiphoton Dissociation of Large Multiply Charged Ions for Biomolecule Sequencing. *Anal. Chem.* **1994,** *66,* 2809–2815.
19. Goolsby, B. J.; Brodbelt, J. S. Characterization of β-lactams by Photodissociation and Collision Activated Dissociation in a Quadrupole Ion Trap. *J. Mass Spectrom.* **1998,** *33,* 705–712.
20. Vartanian, V. H.; Goolsby, B.; Brodbelt, J. S. Identification of Tetracycline Antibiotics by Electrospray Ionization in a Quadrupole Ion Trap. *J. Am. Soc. Mass Spectrom.* **1998,** *9,* 1089–1098.
21. Shi, S. D.-H.; Hendrickson, C. L.; Marshall, A. G.; Siegel, M. M.; Kong, F.; Carter, G. T. Structural Validation of Saccharomyces by High Resolution and High Mass Accuracy Fourier Transform-Ion Cyclotron Resonance Mass Spectrometry and Infrared Multiphoton Dissociation Tandem Mass Spectrometry. *J. Am. Soc. Mass Spectrom.* **1999,** *10,* 1285–1290.
22. Little, D. P.; Aaserud, D. J.; Valaskovic, G. A.; McLafferty, F. W. Sequence Information from 42–108-mer DNAs (Complete for a 50-mer) by Tandem Mass Spectrometry. *J. Am. Chem. Soc.* **1996,** *118,* 9352–9359.
23. Li, W.; Hendrickson, C. L.; Emmett, M. R.; Marshall, A. G. Identification of Intact Proteins in Mixtures by Alternated Capillary Liquid Chromatoraphy Electrospray Ionization and LC ESI Infrared Multiphoton Dissociation Fourier Transform Ion Cyclotron Resonance Mass Spectrometry. *Anal. Chem.* **1999,** *71,* 4397–4402.
24. Hofstadler, S. A.; Sannes-Lowery, K. A.; Griffey, R. H. Infrared Multiphoton Dissociation in an External Ion Reservoir. *Anal. Chem.* **1999,** *71,* 2067–2070.
25. Goolsby, B. J.; Brodbelt, J. S. Analysis of Protonated and Alkali Metal Cationized Aminoglycoside Antibiotics by Collisional Activated Dissociation and Photodissociation in a Quadrupole Ion Trap. *J. Mass Spectrom.* **2000,** *35,* 1011–1024.
26. Goolsby, B. J.; Brodbelt, J. S. Tandem Infrared Multiphoton Dissociation and Collisionally Activated Dissociation Techniques in a Quadrupole Ion Trap. *Anal. Chem.* **2001,** *73,* 1270–1276.
27. Hakansson, K.; Cooper, H. J.; Emmett, M. R.; Costello, C. E.; Marshall, A. G.; Nilsson, C. L. Electron Capture Dissociation and Infrared Multiphoton Dissociation MS/MS of an N-Glycosylated Tryptic Peptide to Yield Complementary Sequence Information. *Anal. Chem.* **2001,** *73,* 4530–4536.
28. Flora, J. W.; Muddiman, D. C. Selective, Sensitive, and Rapid Phosphopeptide Identification in Enzymatic Digests Using ESI-FTICR-MS with Infrared Multiphoton Dissociation. *Anal. Chem.* **2001,** *73,* 3305–3311.
29. Payne, A. H.; Glish, G. L. Thermally Assisted Infrared Multiphoton Photodissociation in a Quadrupole Ion Trap. *Anal. Chem.* **2001,** *73,* 3542–3548.
30. Van Berkel, G. J.; Glish, G. L.; McLuckey, S. A. Electrospray Ionization Combined with Ion Trap Mass Spectrometry. *Anal. Chem.* **1990,** *62,* 1284–1295.
31. Wiley, P. F.; Sigal, M. V.; Weaver, O.; Monahan, R.; Gerzon, K. Erythromycin. XI. Structure of Erythromycin B. *J. Am. Chem. Soc.* **1957,** *79,* 6070–6074.
32. Martin, S. F.unpublished.
33. Martin, S. F.; Hida, T.; Kym, P. R.; Loft, M.; Hodgson, A. The Asymmetric Synthesis of Erythromycin B. *J. Am. Chem. Soc.* **1997,** *119,* 3193–3194.